Charge Fluctuations at the Si-SiO_2 Interface and its Effect on Surface Recombination in Solar Cells

Ruy S. Bonilla[1*], Isabel Al-Dhahir[1], Mingzhe Yu[1], Phillip Hamer[1,2], Pietro P. Altermatt[3]

[1]Department of Materials, University of Oxford, Oxford, OX1 3PH, United Kingdom

[2]School of Photovoltaic and Renewable Energy Engineering, University of New South Wales, Sydney, NSW, 2052, Australia

[3]Trina Solar, State Key Laboratory for Photovoltaic Science and Technology (SKL PVST), Xinbei District, Changzhou, Jiangsu Province 213031, China

Abstract - The Si-SiO_2 interface has and will continue to play a major role in the development of silicon photovoltaic devices. This work presents a detailed examination of how charge at or near this interface influences device performance. New understanding is identified on the effect of charge-induced potential fluctuations at the silicon surface. Such fluctuations have been considered in Si-SiO_2 recombination models previously, where a universal value of electrical potential deviation was used to represent the effect. However, the approach disregards that the variation occurs in the charge concentration rather than the potential. We modify the models to accurately reflect fluctuations in external charge, allowing a precise representation of surface recombination velocity, with self-consistent D_{it}, σ_p, and σ_n parameters. Correctly accounting for these parameters can provide insights into the passivation mechanisms which can aid the development of future devices. Using the corrected model, we find that the effect of charge fluctuation at the Si-SiO_2 interface is significant for the depletion regime to the weak inversion regime. This indicates that surface passivation dielectrics must operate with charge concentrations in excess of $2x10^{12}$ q/cm^2 to avoid these effects. TCAD device simulations show that the efficiency of future PERC cells can improve up to 1% absolute when optimally charged dielectric coatings are applied both at the front and rear surfaces.

Key words: silicon solar cells, silicon dioxide thin films, recombination, surface passivation.

1. Introduction

The physics of the Si-SiO_2 interface has regained substantial attention in recent years. This interest has mainly been sparked by the development of tunnel oxide passivating contacts. The advances reported in the use of SiO_2 nanolayers, most prominently in the work of Fraunhofer ISE [1–3] and ISFH [4–6], has made such layers a prime component in high performance silicon photovoltaic devices. The TOPCon or POLO cell architectures, as they are known in the field, have enabled efficiencies as high as 26% [1–6]. These have been possible by a strong reduction in contact recombination, primarily thanks to the Si-SiO_2 interface. In addition to passivating contacts, Si-SiO_2 has been reported to be vital for aluminium oxide passivation of p-type surfaces [7–9]. An interfacial SiO_2 is required for the alumina layer to build substantial negative charge [10], and in some cases it has been used to control the total negative charge concentration [11,12]. This negative charge in AlO_x passivation layers have made them key in minimising surface losses on p-type Si at the cell's rear, and have thus enabled the ongoing industrial shift to Passivated Emitter and Rear Cell (PERC) technology [13–15]. Most significantly, a thin thermal oxide is nowadays widely used

* Corresponding author: sebastian.bonilla@materials.ox.ac.uk

for passivation in the front of the cell by many Chinese manufacturers. A SiO_2 nanolayer is grown to reduce the interface state density, and thus enhance the surface passivation of PERC cells prior to silicon nitride deposition. This dielectric stack was proposed in the 90s in ISFH [16,17], and it came to prominence as it enabled the development of >24% front contact cells [13,18]. The understanding of the Si-SiO_2 interface has therefore been pivotal for the continuing progress of silicon photovoltaics [19]. These SiO_2 nanolayers will remain a subject of increasing importance among the PV community as higher cell efficiencies are sought.

Despite the significant progress in understanding the Si-SiO_2 interface, many aspects of the charge dynamics at and across this interface remain unknown. In this work, we revise the understanding of the effect of charge at and near a Si-SiO_2 interface. Specifically, new insights are identified on the effect of charge-induced potential fluctuations at the silicon surface. This phenomenon is especially important as it impacts the carrier recombination rate at the Si-SiO_2 interface. Previous reports have stated that such fluctuations arise from (i) charged interfaces states, (ii) random point charges, or (iii) inhomogeneous dielectric fixed charge. Although the effect of potential fluctuations has been widely used in modelling Si-SiO_2 recombination, we find that it has been accounted for wrongly. Experimental results can only be consistently explained by *fluctuations in charge*, rather than surface potential. We demonstrate this by first examining the effect of charge in interface recombination, particularly its dependence on acceptor- and donor-like states. We then propose a new model to account for the charge fluctuations, and use this model to explain experimental results, in the framework of Shockley-Read-Hall (SRH) theory of recombination.

Measurements of effective lifetime have been largely reported as a useful proxy for interface recombination in silicon. To demonstrate the effectiveness of the revised model, we have studied and modelled lifetime experiments in typical oxide and oxide-nitride surface passivation schemes, both from the authors work and from previous reports in the literature. We find that the model of charge fluctuations explains the effect of charges in as-deposited dielectric layers. We also conclude that the effect of charge non-uniformities at the Si-SiO_2 interface is only significant for the depletion to weak inversion regime. This is in contrast to the previous model of potential fluctuations which affects all space charge conditions in a Si surface. Finally, we use Sentaurus TCAD simulations to study how charge fluctuations impact both the front and the rear surfaces of future >23% industrial PERC cells. We see that charge non-uniformities can promote losses in cell performance, and thus optimal surface passivation should operate outside of depletion/inversion regime. We establish the range of charge concentrations that must be present in the dielectrics for the devices to be unaffected by charge non-uniformities.

2. Charge in the SRH model of surface recombination

Following SRH theory [20,21], the surface recombination velocity (SRV) at an interface with a defect distribution $D_{it}(E)$ can be expressed with Girisch's well-known formalism [22]:

$$S = \frac{1}{\Delta n}\int_{Ev}^{Ec} \frac{(n_s p_s - n_i^2)}{\frac{[n_s + n_1(E)]}{v_{thp} D_{it}(E)\sigma_p} + \frac{[p_s + p_1(E)]}{v_{thn} D_{it}(E)\sigma_n}} dE \qquad (1)$$

assuming energy-independent capture cross sections σ_p and σ_n. SRV depends on the trap states factors $n_1(E)$ and $p_1(E)$, and on the concentration of carriers at the interface, n_s and p_s. These concentrations can be controlled by the presence of external charges near the semiconductor surface in the form of (i) charge trapped in the interface defects Q_{it}, (ii) a fixed charge in the dielectric layer, Q_f, or (iii) a biased electrode on top of the dielectric, Q_{gate}. Figure 1 illustrates how these mechanisms can control the surface carrier concentrations n_s

and p_s. In the presence of acceptor and donor-like interface states, pictured in Figure 1.b, a population of electrons is built at the interface such that $Q_{it} < 0$. This in turn induces a mirror space charge from holes near the surface, $p_s > p_{bulk}$, thus a silicon surface charge $Q_{Si} > 0$ for restoring quasi-neutrality.

Figure 1.c pictures the effect of a large concentration of positive charge fixed inside the dielectric layer, $Q_f > 0$. This leads to a mirror charge in the form of an interface $Q_{it} < 0$ and near surface $Q_{Si} < 0$ electron build-up. In an n-type semiconductor as pictured in Figure 1, this corresponds to a heavy accumulation regime ($n_s >> p_s$). A metal gate can finally be used to establish a bias potential and further modify n_s and p_s. For example, a negative gate bias can counteract the positive Q_f, and drive the surface into depletion, or onset inversion ($n_s \approx p_s$), as illustrated in Figure 1.d. If the negative bias is sufficient, the surface can be driven into inversion as shown in Figure 1.e, with ($n_s < p_s$). It is lastly noted that the surface potential parameter ψ_s, pictured in Figure 1, can be used to link the bulk n_{bulk}, p_{bulk}, and surface concentrations, n_s and $p_s$via the simple relationship [23,24]:

$$\frac{Q_{Si}^2}{c} = p\left(e^{-\beta\psi_s} + \beta\psi_s - 1\right) + n\left(e^{\beta\psi_s} - \beta\psi_s - 1\right) \qquad (2)$$

where the constant $c = 2\varepsilon_0\varepsilon_r/q\beta$, and $\beta = q/kT$ in units of eV, assuming low recombination rates such that the quasi-Fermi energy levels are constant in the band-bent region.

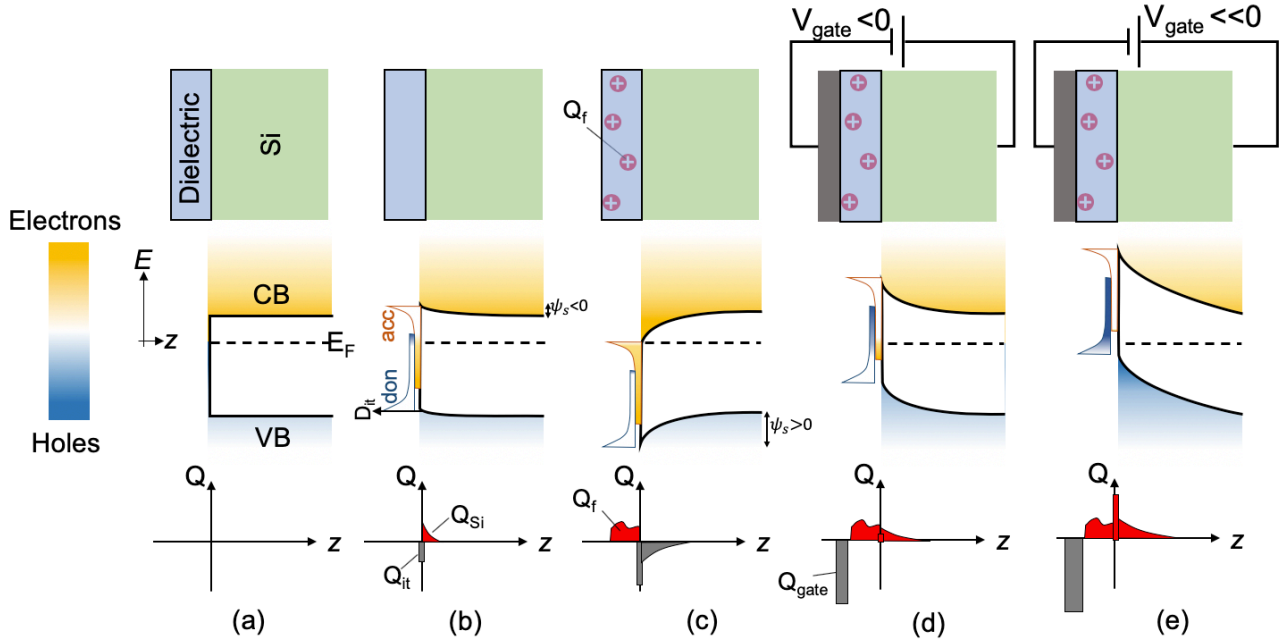

Figure 1. Schematic energy diagram of charge in the semiconductor near surface and interface states, as a product of dielectric and gate charge. (a) The initial neutral state, (b) in the presence of charged donor and acceptor interface states Q_{it}, (c) in the presence of dielectric charged Q_f, (d) effect of charge from a negatively biased metal gate Q_{gate}, and (e) when the gate bias drives the semiconductor surface into inversion. ψ_s denotes the surface potential.

The charge control of n_s and p_s allows the minimisation of SRV via the dependence given in Equation (1). This is known as the field effect or charge assisted passivation mechanism, and its minimum occurs when $n_s\sigma_n = p_s\sigma_p$. If the charge effects are considered as in Figure 1, an exact analytical solutions of the recombination velocity cannot be obtained. A solution can be obtained, however, by an iterative algorithm by Girisch *et al.* [22] and Aberle *et al* [25]. This

procedure is used here to study how SRV is affected by charge-induced changes to ψ_s. Since measurements of effective lifetime τ_{eff} are now widely reported, we also calculate the lifetime τ_{eff} of a symmetric specimen by solving:

$$S_{eff} = \sqrt{D\left(\frac{1}{\tau_{eff}} - \frac{1}{\tau_{bulk}}\right)} \tan\left(\frac{W}{2}\sqrt{\frac{1}{D}\left(\frac{1}{\tau_{eff}} - \frac{1}{\tau_{bulk}}\right)}\right) \quad (3)$$

following Luke and Cheng's [26] formalism, where W is the specimen width and D is the ambipolar carrier diffusion coefficient. In this work we assume Richter's bulk lifetime parametrisation [27], and Klaassen's mobility model [28] (which can be extended to compensated material by Ref [29]), as implemented in PV Lighthouse [30].

Figure 2 illustrates the calculated SRV and τ_{eff} as a function of Q_f, for two values of mid-gap interface state density D_{it}, and typical other parameter values of a Si-SiO_2 interface. Note that the effect of charge in band tail states has been included via the D_{itCB} and D_{itVB} parameters. This follows early reports on the existence of such states [31,32], and recent work pointing out their importance [33,34]. From Figure 2 it is clear that charge at and near the Si-SiO_2 interface can control the surface concentration of carriers, and thus the extent of surface recombination. The ability to control n_s and p_s is limited by the amount of charge stored at the interface Q_{it}. When the available states are increased by an order of magnitude, from 10^{10} to 10^{11} $eV^{-1}cm^{-2}$, the recombination velocity not only increases, but has a lesser dependence on Q_f. This is evident in the broadened peak/valley of Figure 2. a/b. These characteristics point to the importance of fluctuations in interface trapped charge as it can prevent the effective exploitation of field effect passivation, and therefore must be correctly accounted for.

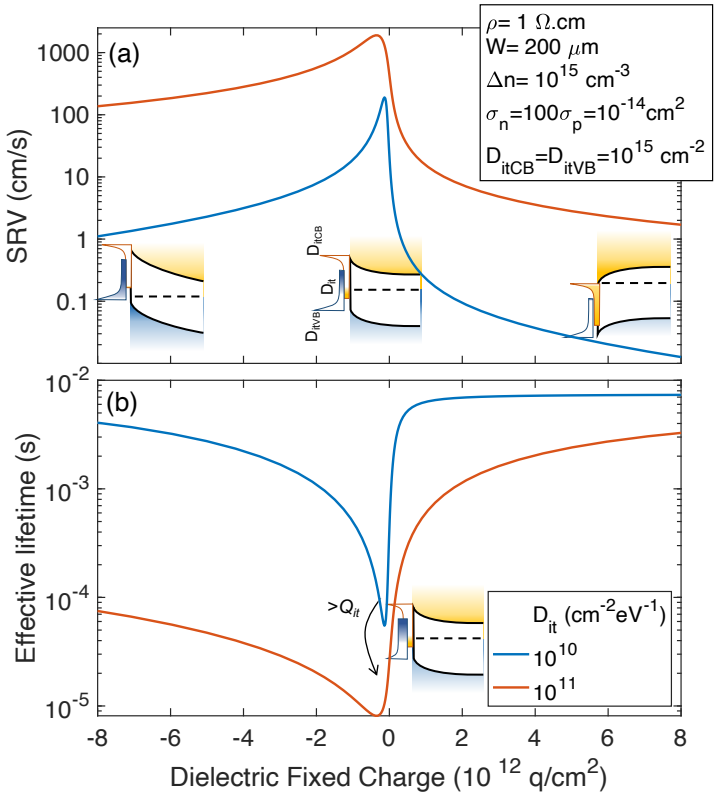

Figure 2. Calculated (a) surface recombination velocity and (b) effective lifetime as function of dielectric charge for typical parameters in a Si-SiO_2 interface, for 1 Ωcm n-type silicon. Insets illustrate the energy band diagrams for the different regimes, highlighting interface charge and carrier concentrations.

3. From potential fluctuations to charge fluctuations

Glunz *et al.* later complemented Girisch and Aberle's model by introducing a term that accounts for random point and inhomogeneous charges [35]. Such nonuniform charge has been attributed to oxide or interface trap states, and a detailed report on the origin of this phenomenon can be found in Nicollian and Brews' book [36]. Glunz accounted for charge non-uniformities using a Gaussian distribution of surface potentials with standard deviation σ_s:

$$S_\sigma = \int_{-\infty}^{\infty} S\left(D_{it}, \sigma_n, \sigma_p, Q_f, \psi_s\right) * \frac{1}{\sigma_s\sqrt{2\pi}} \exp\left(\frac{(\psi_s - \psi_{s0})^2}{2\sigma_s^2}\right) d\psi_s \quad (4)$$

This addition has been later adopted to describe recombination at other dielectric-semiconductor systems, e.g. in [37–40]. It is most relevant when surface passivation is controlled using external surface charge, caused by either the dielectric or a gate electrode.

The results of adding this component to the model is shown in Figure 3 for a typical Si-SiO_2 interface. A value of σ_s=2kT/q is chosen following that reported in [35]. It is clear that variations in the surface potential, using the approach in [35–37], strongly influence the recorded SRV and lifetime behaviour. If the inhomogeneity in potential is high, the dependence of lifetime on surface charge is largely reduced (dotted lines). This reduced dependence is predicted by Glunz *et al* for both small and large charge densities, and the maximum achievable lifetimes at high charges are much reduced.

However, the origin of the fluctuations is not a fluctuation of ψ_s, but fluctuations of the fixed charge Q_f and, to a far smaller extent, of the trapped charge Q_f. Figure 2 shows that, for a given fluctuation of Q_f, the induced fluctuation of ψ_s, is smaller when the average Q_f is large. Hence, σ_s cannot be a constant in Glunz et al.'s model. By assigning a single, universal value of σ_s this aspect is overlooked and leads to a strong widening of the observed lifetime-to-charge dependence. To alleviate this, we propose that the fluctuation is instead assigned to the external charge Q_f, and not to ψ_s, and is computed for each iteration of Girisch and Aberle's algorithm using a standard deviation σ_q:

$$S_\sigma = \int_{-\infty}^{\infty} S\left(D_{it}, \sigma_n, \sigma_p, Q_f, \psi_s\right) * \frac{1}{\sigma_q\sqrt{2\pi}} \exp\left(\frac{\left(Q_f - Q_{f0}\right)^2}{2\sigma_q^2}\right) dQ_f \quad (5)$$

The calculations are illustrated by the dashed lines in Figure 3. Here, a standard deviation in charge σ_q =5x10^{11} q/cm^2 is used since it reflect a typicial charge density in oxide-nitride passivation films [41]. The main difference to Glunz *et al*. is that the broadening is now only observed for low charge concentrations where the surface is in depletion/inversion. This occurs near the maximum recombination, which makes this effect important when using the lifetime minima as a measure of the amount of change in chemical passivation, as has been done e.g. in [8,39,42–44]. Most importantly, it does not influence the maximum attainable lifetimes for the charge concentrations often attained in dielectric coatings (1-6x10^{12} q/cm^2).

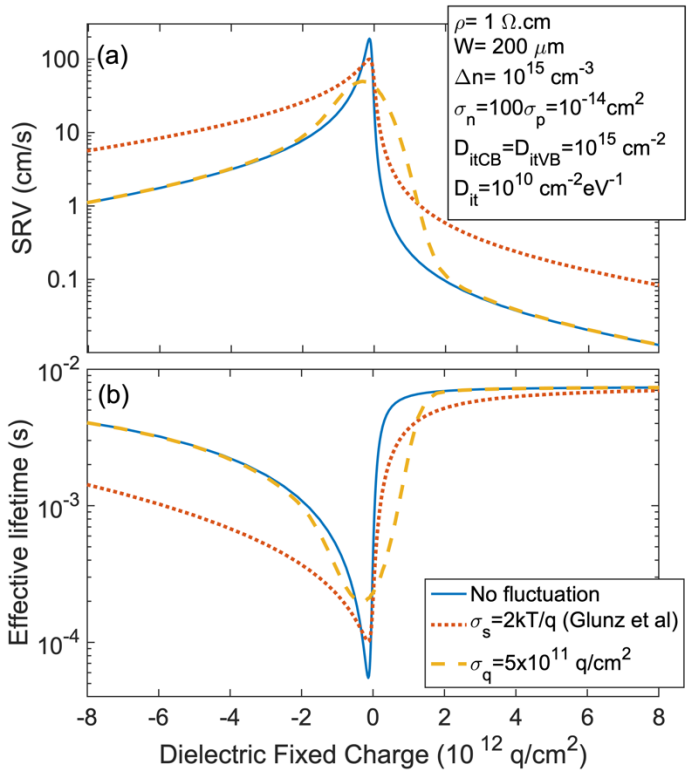

Figure 3. Calculated (a) SRV and (b) effective lifetime as function of dielectric charge using the traditional model of Glunz et al. [35] and our new model of charge fluctuations, for the indicated settings of surface model parameters.

4. Modelling silicon lifetime data

The modelling approach introduced in Sections 2 and 3 is used now to experimentally evaluate the extent to which surface potential fluctuations can affect the recombination at the Si-SiO_2 interface. For this, 200 µm thick n-type, 1 Ωcm float-zone silicon wafers were oxidised in a dry atmosphere to ~100 nm thickness, followed by a forming gas anneal (FGA), and PECVD SiN_x deposition. The surface recombination at each stage: (a) after oxidation, (b) after FGA, and (c), after SiN_x deposition, was monitored by using a transparent PEDOT:PSS gate electrode to control ψ_s, and modulate n_s and p_s. Effective lifetime was acquired as a function of the surface potential applied to the gate electrode on the front and rear dielectrics, using a Sinton WCT-120 instrument. This methodology is described in detail in [45].

Figure 4.a shows τ_{eff} at $\Delta n=10^{15}$ cm^{-3} for these three specimens. The solid lines represent the least-square fits obtained following our new model including the effect of charge in the band tails [33]. The model parameters are listed in Table 1. From the fits it is clear that an accurate description of the measurements is possible with this analytical model. The least square fit to Glunz et al.'s model is represented by the dashed line. It requires a reduction in the band tails well below values reported in the literature [33,34], and results in a rather poor model for σ_s between 0.5 to 3 kT/q, primarily due to the overestimated effect for large band-bending conditions. As expected, from the model fit we observe that a thermal oxide-silicon interface exhibits a reduction in interface state density upon FGA and nitride deposition due to hydrogenation [46–49]. These reductions are largely responsible for the lower capture rates observed, as the cross sections decreased marginally, considering $S_{n0} = v_{th}D_{it}\sigma_n$, and $S_{p0} = v_{th}D_{it}\sigma_p$. The broadening of the curves observed can be explained by the fluctuations in charge given by σ_q. Correctly accounting for this effect can provide insights into the

passivation mechanisms. For example, at the Si-SiO_2 an improvement in chemical passivation was observed, and with this model it could primarily be linked to reductions in interface state density, with a minor contribution from lower capture cross sections.

To demonstrate the effectiveness of this model, we have also simulated SRV data reported by Schmidt [43] and Dingemans [8]. The original data and the fits are shown in Figure 4.b, with the parameters listed in Table 1. The key advantage of accounting for fluctuations in charge instead of band bending is that the model parameters used are self-consistent with values of D_{it}, σ_p, and σ_n previously studied using impedance spectroscopy measurements [17,37,50–52]. These models show that charge fluctuations in both nitride and alumina films can be severe, and thus the final charge in the film should promote band-bending outside of the depletion regime. Table 1 also lists the found capture ratios k = σ_n/σ_p. The difference in k-factor of SiO_2 among the three experiments in this paper and that in [8] can be explained by the U_M defects [32]. They dominate after hydrogenation over the P_L defects and have a higher k-factor [53], which can be explained by spin-induced triplet recombination [54], which slows the relaxation during DLTS measurements [55]. The difference in k-factor of SiN_x between [43] and [8] can be explained by the prevalence of defect A or B [56].

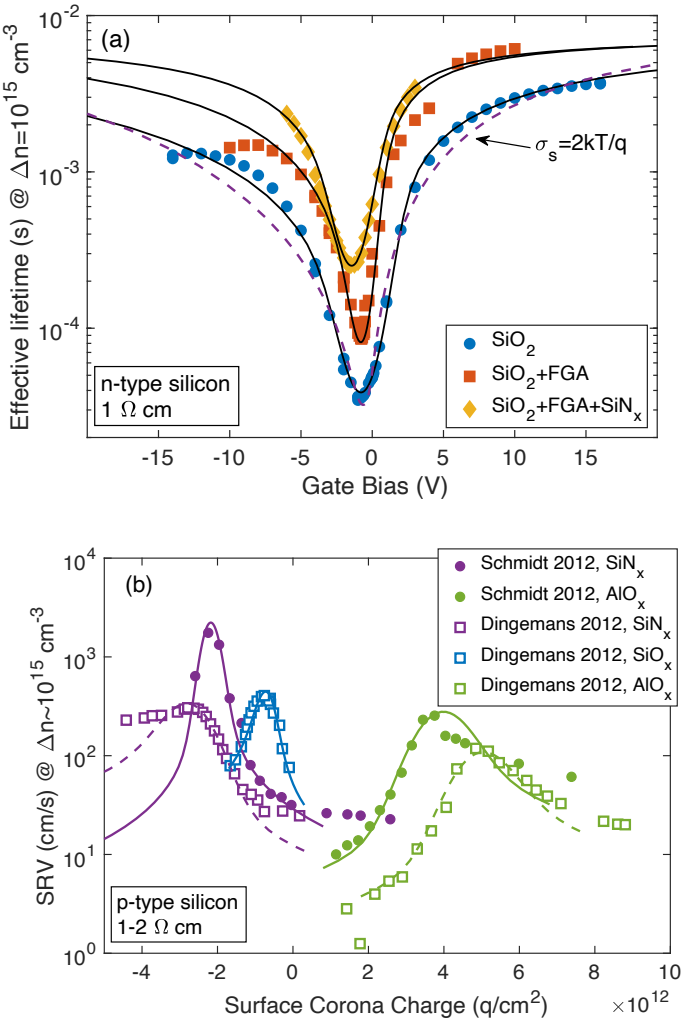

Figure 4. (a) Measured effective lifetime as a function of gate potential on the surface of the oxide, or oxide/nitride passivation layers (symbols). Solid lines indicate fits obtained using new model. Dashed line indicates the best fit using the old model. (b) Previous reports of SRV as a function of surface charge fitted with the model here developed.

Table 1. Model parameters used to fit empirical data in this work, and that of references [8,43]. Last row lists the parameters that best fit observations in SiO_2 using the old model.

	SiO_2	**SiO_2+FGA**	**SiO_2+FGA +SiN_x**	**SiN_x** [43]	**SiN_x** [8]	**SiO_x** [8]	**AlO_x** [43]	**AlO_x** [8]
D_{it} ($cm^{-2}eV^{-1}$)	10^{11}	$5x10^{10}$	10^{10}	10^{11}	10^{11}	$4x10^{11}$	10^{11}	10^{11}
σ_p (10^{-16} cm^2)	1.1	0.576	1.74	65.5	1.96	0.327	17.4	2.62
σ_n (10^{-16} cm^2)	8.7	7.7	10.5	43.6	5.24	0.87	4.36	0.7
k = σ_n/σ_p	7.9	13.4	6.0	0.67	2.65	2.66	0.25	0.26
Q_{f0} (10^{11} q/cm^2)	2.2	2.2	2.6	22	26	7	-38	-48
σ_q (10^{11} q/cm^2)	2	1	1.2	2	5	1	6	6
D_{itVB},D_{itCB} (10^{14} cm^{-2})	8, 20	8, 20	10, 30	10,10	200,80	80,80	80, 100	80, 100
σ_s (q/cm^2)	2kT/q							
D_{itVB},D_{itCB}(10^{14} cm^{-2})	0.8, 2							

5. Effect of dielectric charge fluctuations on cell performance

We quantified the effects of charge and its fluctuations in the performance of PERC cells with simulations in Sentaurus TCAD [57]. The cells parameters were adapted from those reported in the literature to model the expected performance of ~23.5-24% in future PERC cells [58–60]. A full account of the cell parameters is provided in the online supplementary materials. Figure 5 illustrates the results of such simulations. Figure 5.a plots the conversion efficiency degradation occurring as a result of reduced front and rear dielectric charge. In high efficiency cells, the lack of charge can account for a loss in performance of 1.2 % absolute due to front recombination, and as much as 4% absolute due to rear recombination. It is therefore clear that optimal surface passivation dielectrics must provide a substantial concentration of charge in order to mitigate surface recombination losses. Such charged dielectrics must provide a silicon surface space charge in excess of $2x10^{12}$ q/cm^2. When industrial dielectrics with $Q\sim10^{12}$ q/cm^2 are optimised to concentrations $\sim10^{13}$ q/cm^2, top-right region in Figure 5.a, they can provide gains in efficiency of ~1% absolute.

When fluctuations in charge are considered, the dependence of efficiency on charge is modified, as indicated by the dashed lines in Figure 5.a. For the front surface this effect is primarily beneficial in the low charge concentrations $Q < 5x10^{11}$ q/cm^2, since the fluctuation into higher charge will promote passivation. For higher charges like $Q > 5x10^{11}$ q/cm^2 in the front surface, the efficiency is negligibly lower than that in the absence of charge non-uniformities. For the rear surface the effect is stronger. Similarly, for low charge $Q < 10^{11}$ q/cm^2 the net effect is an increased efficiency. However, when the total charge continues to increase at the rear, fluctuations will hinder the passivation and lower the efficiency in the range $10^{11} < Q < 2x10^{12}$ q/cm^2. It is sometimes observed in mass production of PERC cells that the rear charge drops below $2x10^{12}$ q/cm^2 and then leads to substantially lower cell efficiencies. This provides a second reason for the dielectric charge to be optimised to values $Q > 2x10^{12}$ q/cm^2. In such range excellent field effect passivation is provided, without hinderance from charge fluctuations. The importance of enhancing the field effect passivation has also been increasingly reported in the literature [61–64].

Figure 5.b illustrates the current-voltage (IV) characteristics of the modelled cells for three points indicated in Figure 5.a. These IV curves evidence the loss in different performance

metrics when the front and rear charge are removed. In absence of front charge the performance loss is primarily related to a lowering in the open-circuit voltage due to increase front surface recombination. For the rear surface, lack of charge causes reductions both in the open-circuit voltage and short-circuit current. This indicates a reduction not just in the quasi-fermi level separation, but also the collection efficiency of the device because high recombination rates at the rear hinder carrier collection from the rear to the front junction. Optimal PERC cells must accomplish large concentrations of charge both in the front and rear surfaces.

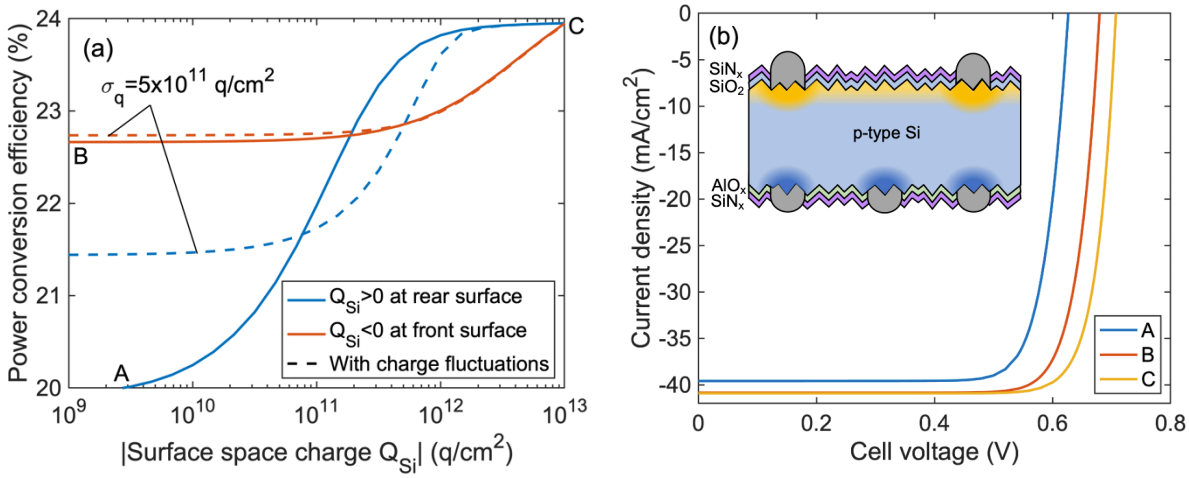

Figure 5. (a) Sentaurus Device simulations of PERC cell performance as a function of front and rear dielectric charge. Charge in Sentaurus is fully mirrored as space charge Q_{Si} hence the x-axis has been labelled correspondingly. When front charge is varied, the rear charge is constant at Q_{Si} =10^{13} q/cm^2, and vice versa. (b) Current-voltage characteristics for the cells at points A, B and C in figure (a). Inset pictures the schematic structure of the cell modelled in this work.

6. Conclusions

This work presented new insights into the physics of the Si-SiO$_2$ interface, especially with regards to the effects of charge fluctuations at or near this interface. While fixed charge has been known to play an important role in the performance of Si devices, the effect of charge-induced potential fluctuations has been previously misinterpreted. Here, the non-uniformities are accounted for by introducing a model for fluctuations in charge, rather than surface potential. This model is used then to explain consistently experimental results on lifetime and recombination in passivated silicon specimens. It is concluded that the effect of charge non-uniformities is significant for the depletion regime to weak inversion regime, and thus final devices should aim to operate outside of such regime with Q>2x10^{12} q/cm^2. In addition, the physical importance of this model must be taken into account when effective lifetime measurements are used to extract interface recombination parameters, .e.g. for calculating the $S_0 = v_{th} D_{it} \sigma$ term. Charge fluctuations can blur the identification of the weak inversion regime and thus render erroneous interpretations. This model must also be included in interface characterisation using the conductance-voltage method of Nicollian and Goetzberger [36,65,66]. Lastly, Senturus TCAD simulations show that charge fluctuations can impact both the front and the rear surfaces of high efficiency PERC cells, with the most important dependence in the rear surface. Excellent dielectric field effect passivation using Q~10^{13} q/cm^2 can lead to improvements of 1% absolute in PERC cell efficiency.

7. Supporting materials

All details of the Sentaurus TCAD simulations and the Girisch/Aberle algorithm are described in the online supplementary materials. The Matlab scripts for calculation of surface recombination and effective lifetime are openly available on https://github.com/OxfordInterfacesLab. All experimental data published in this article can be downloaded from http://ora.ox.ac.uk.

8. Acknowledgments

P. Hamer acknowledges the funding support from ACAP as a postdoctoral fellow. P.P. Altermatt acknowledges support from Black Silicon Photovoltaics grant EP/R005303/1. R. S. Bonilla is recipient of a Royal Academy of Engineering Research Fellowship, and acknowledges the support from ESPRC Postdoctoral Fellowship EP/M022196/1.

9. References

[1] S.W. Glunz, F. Feldmann, A. Richter, M. Bivour, C. Reichel, H. Steinkemper, J. Benick, M. Hermle, The Irresistible Charm of a Simple Current Flow Pattern – 25 % With a Solar Cell Featuring a Full-Area Back Contact, Proceedings of the 31st European Photovoltaic Solar Energy Conference and Exibition. (2015) 259–263. doi:10.4229/EUPVSEC20152015-2BP.1.1.

[2] F. Feldmann, M. Bivour, C. Reichel, H. Steinkemper, M. Hermle, S.W. Glunz, Tunnel oxide passivated contacts as an alternative to partial rear contacts, Solar Energy Materials and Solar Cells. 131 (2014) 46–50. doi:10.1016/j.solmat.2014.06.015.

[3] F. Feldmann, M. Bivour, C. Reichel, M. Hermle, S.W. Glunz, Passivated rear contacts for high-efficiency n-type Si solar cells providing high interface passivation quality and excellent transport characteristics, Solar Energy Materials and Solar Cells. 120 (2014) 270–274. doi:10.1016/j.solmat.2013.09.017.

[4] C. Hollemann, F. Haase, M. Rienäcker, V. Barnscheidt, J. Krügener, N. Folchert, R. Brendel, S. Richter, S. Großer, E. Sauter, J. Hübner, M. Oestreich, R. Peibst, Separating the two polarities of the POLO contacts of an 26.1%-efficient IBC solar cell, Scientific Reports. 10 (2020). doi:10.1038/s41598-019-57310-0.

[5] C. Hollemann, F. Haase, S. Schäfer, J. Krügener, R. Brendel, R. Peibst, 26.1%-efficient POLO-IBC cells: Quantification of electrical and optical loss mechanisms, Progress in Photovoltaics: Research and Applications. 27 (2019) 950–958. doi:10.1002/pip.3098.

[6] S. Schäfer, F. Haase, C. Hollemann, J. Hensen, J. Krügener, R. Brendel, R. Peibst, 26%-Efficient and 2 Cm Narrow Interdigitated Back Contact Silicon Solar Cells With Passivated Slits on Two Edges, Solar Energy Materials and Solar Cells. 200 (2019). doi:10.1016/j.solmat.2019.110021.

[7] B. Hoex, J. Schmidt, P. Pohl, M.C.M. van de Sanden, W.M.M. Kessels, Silicon surface passivation by atomic layer deposited Al2O3, Journal of Applied Physics. 104 (2008) 044903. doi:10.1063/1.2963707.

[8] G. Dingemans, W.M.M. Kessels, Status and prospects of Al2O3-based surface passivation schemes for silicon solar cells, Journal of Vacuum Science & Technology A: Vacuum, Surfaces, and Films. 30 (2012) 40802. doi:10.1116/1.4728205.

[9] S. Duttagupta, F. Lin, K.D. Shetty, A.G. Aberle, B. Hoex, Excellent boron emitter passivation for high-efficiency Si wafer solar cells using AlOx/SiNx dielectric stacks deposited in an industrial inline plasma reactor, Progress in Photovoltaics: Research

and Applications. 21 (2013) 760–764. doi:10.1002/pip.1259.

[10] J. Schmidt, A. Merkle, R. Brendel, B. Hoex, M.C.M. Van De Sanden, W.M.M. Kessels, Surface passivation of high-efficiency silicon solar cells by atomic-layer-deposited Al2O3, Progress in Photovoltaics: Research and Applications. 16 (2008) 461–466. doi:10.1002/pip.823.

[11] D. Hiller, P.M. Jordan, K. Ding, M. Pomaska, T. Mikolajick, D. König, Deactivation of silicon surface states by Al-induced acceptor states from Al-O monolayers in SiO 2, Journal of Applied Physics. 125 (2019). doi:10.1063/1.5054703.

[12] D. Hiller, J. Göttlicher, R. Steininger, T. Huthwelker, J. Julin, F. Munnik, M. Wahl, W. Bock, B. Schoenaers, A. Stesmans, D. König, Structural Properties of Al-O Monolayers in SiO2 on Silicon and the Maximization of Their Negative Fixed Charge Density, ACS Applied Materials and Interfaces. 10 (2018) 30495–30505. doi:10.1021/acsami.8b06098.

[13] A. Blakers, Development of the PERC Solar Cell, IEEE Journal of Photovoltaics. 9 (2019) 629–635. doi:10.1109/JPHOTOV.2019.2899460.

[14] M.A. Green, The Passivated Emitter and Rear Cell (PERC): From conception to mass production, Solar Energy Materials and Solar Cells. 143 (2015) 190–197. doi:10.1016/J.SOLMAT.2015.06.055.

[15] P.P. Altermatt, Y. Chen, Y. Yang, Z. Feng, Riding the workhorse of the industry: PERC, Photovoltaics International. 41 (2018) 46–54.

[16] J. Schmidt, T. Lauinger, A.G. Aberle, R. Hezel, Record low surface recombination velocities on low-resistivity silicon solar cell substrates, in: Conference Record of the Twenty Fifth IEEE Photovoltaic Specialists Conference - 1996, IEEE, 1996: pp. 413–416. doi:10.1109/PVSC.1996.564031.

[17] J. Schmidt, A.G. Aberle, Carrier recombination at silicon–silicon nitride interfaces fabricated by plasma-enhanced chemical vapor deposition, Journal of Applied Physics. 85 (1999) 3626–3633. doi:10.1063/1.369725.

[18] J. Zhao, A. Wang, M.A. Green, 24.5% Efficiency silicon PERT cells on MCZ substrates and 24·7% efficiency PERL cells on FZ substrates, Progress in Photovoltaics: Research and Applications. 7 (1999) 471–474. doi:10.1002/(SICI)1099-159X(199911/12)7:6<471::AID-PIP298>3.0.CO;2-7.

[19] S.W. Glunz, F. Feldmann, SiO2 surface passivation layers – a key technology for silicon solar cells, Solar Energy Materials and Solar Cells. 185 (2018) 260–269. doi:10.1016/j.solmat.2018.04.029.

[20] W. Shockley, W.T. Read, Statistics of the Recombinations of Holes and Electrons, Physical Review. 87 (1952) 835–842.

[21] R.N. Hall, Electron-Hole Recombination in Germanium, Physical Review. 87 (1952) 387.

[22] R.B.M. Girisch, R.P. Mertens, R.F. Dekeersmaecker, R.F. De Keersmaecker, Determination of Si-SiO2 Interface Recombination Parameters using a Gate-Controlled Point-Junction Diode under Illumination, Ieee Transactions on Electron Devices. 35 (1988) 203–222. doi:10.1109/16.2441.

[23] A.S. Grove, D.J. Fitzgerald, Surface effects on p-n junctions: Characteristics of surface space-charge regions under non-equilibrium conditions, Solid-State Electronics. 9

(1966) 783–806. doi:10.1016/0038-1101(66)90118-3.

[24] C.E. Young, Extended curves of the space charge, electric field, and free carrier concentration at the surface of a semiconductor, and curves of the electrostatic potential inside a semiconductor, Journal of Applied Physics. 32 (1961) 329–332. doi:10.1063/1.1736007.

[25] A.G. Aberle, S. Glunz, W. Warta, Impact of illumination level and oxide parameters on Shockley-Read-Hall recombination at the Si-SiO2 interface, Journal of Applied Physics. 71 (1992) 4422–4431. doi:10.1063/1.350782.

[26] K.L. Luke, L.-J. Cheng, Analysis of the interaction of a laser pulse with a silicon wafer: Determination of bulk lifetime and surface recombination velocity, Journal of Applied Physics. 61 (1987) 2282. http://link.aip.org/link/?JAPIAU/61/2282/1 (accessed August 20, 2012).

[27] A. Richter, S.W. Glunz, F. Werner, J. Schmidt, A. Cuevas, Improved quantitative description of Auger recombination in crystalline silicon, Physical Review B. 86 (2012) 165202. doi:10.1103/PhysRevB.86.165202.

[28] D.B.M. Klaassen, A unified mobility model for device simulation—II. Temperature dependence of carrier mobility and lifetime, Solid-State Electronics. 35 (1992) 961–967. doi:10.1016/0038-1101(92)90326-8.

[29] F. Schindler, M. Forster, J. Broisch, J. Schön, J. Giesecke, S. Rein, W. Warta, M.C. Schubert, Towards a unified low-field model for carrier mobilities in crystalline silicon, Solar Energy Materials and Solar Cells. 131 (2014) 92–99. doi:10.1016/j.solmat.2014.05.047.

[30] www.pvlighthouse.com.au, PV LightHouse, (2017).

[31] H. Flietner, W. Füssel, N.D. Sinh, H. Angermann, Density of states and relaxation spectra of etched, H-terminated and naturally oxidized Si-surfaces and the accompanied defects, Applied Surface Science. 104–105 (1996) 342–348. doi:10.1016/S0169-4332(96)00168-7.

[32] W. Füssel, M. Schmidt, H. Angermann, G. Mende, H. Flietner, Defects at the Si/SiO2 interface: Their nature and behaviour in technological processes and stress, Nuclear Instruments and Methods in Physics Research, Section A: Accelerators, Spectrometers, Detectors and Associated Equipment. 377 (1996) 177–183. doi:10.1016/0168-9002(96)00205-7.

[33] R.S. Bonilla, P.R. Wilshaw, On the c-Si/SiO2 interface recombination parameters from photo-conductance decay measurements, Journal of Applied Physics. 121 (2017) 135301. doi:10.1063/1.4979722.

[34] Z. Xin, S. Duttagupta, M. Tang, Z. Qiu, B. Liao, A.G. Aberle, R. Stangl, An Improved Methodology for Extracting the Interface Defect Density of Passivated Silicon Solar Cells, IEEE Journal of Photovoltaics. 6 (2016) 1080–1089. doi:10.1109/JPHOTOV.2016.2576685.

[35] S.W. Glunz, D. Biro, S. Rein, W. Warta, Field-effect passivation of the SiO2Si interface, Journal of Applied Physics. 86 (1999) 683–691. doi:10.1063/1.370784.

[36] E.H. Nicollian, J.R. Brews, MOS Physics and Technology, Wiley, New York, 1982.

[37] L.E. Black, New Perspectives on Surface Passivation: Understanding the Si-Al2O3 Interface, Springer International Publishing, Cham, 2016. doi:10.1007/978-3-319-

32521-7.

[38] S. Mack, A. Wolf, C. Brosinsky, S. Schmeisser, A. Kimmerle, P. Saint-Cast, M. Hofmann, D. Biro, Silicon surface passivation by thin thermal Oxide/PECVD layer stack systems, IEEE Journal of Photovoltaics. 1 (2011) 135–145. doi:10.1109/JPHOTOV.2011.2173299.

[39] F. Werner, A. Cosceev, J. Schmidt, Interface recombination parameters of atomic-layer-deposited Al 2O 3 on crystalline silicon, in: Journal of Applied Physics, 2012. doi:10.1063/1.3700241.

[40] S. Garud, N. Gampa, T.G. Allen, R. Kotipalli, D. Flandre, M. Batuk, J. Hadermann, M. Meuris, J. Poortmans, A. Smets, B. Vermang, Surface Passivation of CIGS Solar Cells Using Gallium Oxide, Physica Status Solidi (A) Applications and Materials Science. 215 (2018). doi:10.1002/pssa.201700826.

[41] R.S. Bonilla, C. Reichel, M. Hermle, P.R. Wilshaw, On the location and stability of charge in SiO2/SiNx dielectric double layers used for silicon surface passivation, Journal of Applied Physics. 115 (2014) 144105. doi:10.1063/1.4871075.

[42] R.S. Bonilla, C. Reichel, M. Hermle, P.R. Wilshaw, Extremely low surface recombination in 1 Ω cm n-type monocrystalline silicon, Physica Status Solidi (RRL) - Rapid Research Letters. 1 (2016) 1–5. doi:10.1002/pssr.201600307.

[43] J. Schmidt, F. Werner, B. Veith, D. Zielke, S. Steingrube, P.P. Altermatt, S. Gatz, T. Dullweber, R. Brendel, Advances in the Surface Passivation of Silicon Solar Cells, Energy Procedia. 15 (2012) 30–39. doi:10.1016/j.egypro.2012.02.004.

[44] B. Veith, T. Dullweber, M. Siebert, C. Kranz, F. Werner, N.P. Harder, J. Schmidt, B.F.P. Roos, T. Dippell, R. Brendel, Comparison of ICP-AlOx and ALD-Al2O3 layers for the rear surface passivation of c-Si solar cells, in: Energy Procedia, 2012: pp. 379–384. doi:10.1016/j.egypro.2012.07.080.

[45] R.S. Bonilla, Controlling Surface Carrier Density via a PEDOT:PSS Gate: An Application to the Study of Silicon-Dielectric Interface Recombination, Solar RRL. (2018) 1800172. doi:10.1002/solr.201800172.

[46] M.J. Kerr, J. Schmidt, A. Cuevas, J.H. Bultman, Surface recombination velocity of phosphorus-diffused silicon solar cell emitters passivated with plasma enhanced chemical vapor deposited silicon nitride and thermal silicon oxide, Journal of Applied Physics. 89 (2001) 3821–3826.

[47] J. Schmidt, M. Kerr, Highest-quality surface passivation of low-resistivity p-type silicon using stoichiometric PECVD silicon nitride, Solar Energy Materials and Solar Cells. 65 (2001) 585–591. doi:10.1016/S0927-0248(00)00145-8.

[48] R.S. Bonilla, F. Woodcock, P.R. Wilshaw, Very low surface recombination velocity in n-type c-Si using extrinsic field effect passivation, Journal of Applied Physics. 116 (2014) 054102. doi:10.1063/1.4892099.

[49] R.S. Bonilla, P.G. Hamer, P.R. Wilshaw, Lowest surface recombination in n-type oxidised crystalline silicon by means of extrinsic field effect passivation, in: EUPVSEC, Munich, Germany, 2016: pp. 707–710. doi:10.4229/EUPVSEC20162016-2AV.2.13.

[50] S. Dauwe, Low-temperature Surface Passivation of Crystalline Silicon and its Application to the Rear Side of Solar Cells, PhD Thesis, Univeristy of Hannover, 2004.

[51] S. Dauwe, L. Mittelstadt, A. Metz, J. Schmidt, R. Hezel, Low-Temperature Rear Surface

Passivation Schemes for >20% Efficient Silicon Solar Cells, in: 3rd World Conference on Photovoltaic Energy Conversion, 2003: p. 1395.

[52] G. Dingemans, Nanolayer surface passivation schemes for silicon solar cells, Technische Universiteit Eindhoven, 2011.

[53] J. Albohn, W. Füssel, N.D. Sinh, K. Kliefoth, W. Fuhs, Capture cross sections of defect states at the Si/SiO2 interface, Journal of Applied Physics. 88 (2000) 842–849. doi:10.1063/1.373746.

[54] F. Friedrich, C. Boehme, K. Lips, Triplet recombination at P b centers and its implications for capture cross sections, Journal of Applied Physics. 97 (2005). doi:10.1063/1.1851593.

[55] R. Beyer, H. Burghardt, I. Thurzo, D.R.T. Zahn, T. Geßner, Deconvolution of the transient response of (1 0 0) Si/SiO2 semiconductor-insulator interface states according to small pulse excitation: Evidence of different branches of charge transition, Solid-State Electronics. 44 (2000) 1463–1470. doi:10.1016/S0038-1101(00)00064-2.

[56] J. Schmidt, F.M. Schuurmans, W.C. Sinke, S.W. Glunz, A.G. Aberle, Observation of multiple defect states at silicon–silicon nitride interfaces fabricated by low-frequency plasma-enhanced chemical vapor deposition, Applied Physics Letters. 71 (1997) 252. doi:10.1063/1.119512.

[57] www.synopsys.com/silicon/tcad.html, Device Simulation Tools - Sentaurus, Synopsys Inc - Sentaurus Device TCAD, (2017). (n.d.). http://www.synopsys.com/TOOLS/TCAD/DEVICESIMULATION/Pages/default.aspx (accessed August 20, 2012).

[58] A. Fell, P.P. Altermatt, A Detailed Full-Cell Model of a 2018 Commercial PERC Solar Cell in Quokka3, IEEE Journal of Photovoltaics. (2018) 1–6. doi:10.1109/JPHOTOV.2018.2863548.

[59] B. Min, M. Müller, H. Wagner, G. Fischer, R. Brendel, P.P. Altermatt, H. Neuhaus, M. Muller, H. Wagner, G. Fischer, R. Brendel, P.P. Altermatt, H. Neuhaus, M. Müller, H. Wagner, G. Fischer, R. Brendel, P.P. Altermatt, H. Neuhaus, A Roadmap Toward 24% Efficient PERC Solar Cells in Industrial Mass Production, IEEE Journal of Photovoltaics. 7 (2017) 1541–1550. doi:10.1109/JPHOTOV.2017.2749007.

[60] A. Fell, K.R. McIntosh, P.P. Altermatt, G.J.M. Janssen, R. Stangl, A. Ho-Baillie, H. Steinkemper, J. Greulich, M. Muller, B. Min, K.C. Fong, M. Hermle, I.G. Romijn, M.D. Abbott, Input Parameters for the Simulation of Silicon Solar Cells in 2014, IEEE Journal of Photovoltaics. 5 (2015) 1250–1263. doi:10.1109/JPHOTOV.2015.2430016.

[61] T.C. Kho, S.C. Baker-Finch, K.R. McIntosh, The study of thermal silicon dioxide electrets formed by corona discharge and rapid-thermal annealing, Journal of Applied Physics. 109 (2011) 053108. doi:10.1063/1.3559260.

[62] R.S. Bonilla, P.R. Wilshaw, Stable field effect surface passivation of n-type Cz silicon, in: Energy Procedia - Proceedings of the 3rd Silicon PV Conference, Elsevier, Hamelin, Germany, 2013: pp. 816–822. doi:10.1016/j.egypro.2013.07.351.

[63] T. Niewelt, A. Richter, T.C. Kho, N.E. Grant, R.S. Bonilla, B. Steinhauser, J.I. Polzin, F. Feldmann, M. Hermle, J.D. Murphy, S.P. Phang, W. Kwapil, M.C. Schubert, Taking monocrystalline silicon to the ultimate lifetime limit, Solar Energy Materials and Solar Cells. 185 (2018) 252–259. doi:10.1016/j.solmat.2018.05.040.

[64] T.C. Kho, K. Fong, K. McIntosh, E. Franklin, N. Grant, M. Stocks, S.P. Phang, Y. Wan, E.C. Wang, K. Vora, Z. Ngwe, A. Blakers, Exceptional silicon surface passivation by an ONO dielectric stack, Solar Energy Materials and Solar Cells. 189 (2019) 245–253. doi:10.1016/j.solmat.2018.05.061.

[65] E.H. Nicollian, A. Goetzberger, The Si-SiO2 Interface — Electrical Properties as Determined by the Metal-Insulator-Silicon Conductance Technique, Bell System Technical Journal. 46 (1967) 1055–1133. doi:10.1002/j.1538-7305.1967.tb01727.x.

[66] E.H. Nicollian, A. Goetzberger, MOS Conductance Technique for Measuring Surface State Parameters, Applied Physics Letters. 7 (1965) 216. doi:10.1063/1.1754385.